Topology Optimization of Microwave Devices with Thin Structure

Takuto Jibiki[1,2], Takeshi Kawasaki[2], Masahiro Tanomura[2], and Hajime Igarashi[1]

[1]Graduate School of Information Science and Technology, Hokkaido University, Sapporo 060-0814, Japan
[2]Sumitomo Electric Industries, LTD. 1, Taya-cho, Sakae-ku, Yokohama 244-8588, Japan

This paper presents a topology optimization of a microstrip bandpass filter (BPF) based on the geometry projection method that can represent thin metals and air gaps. A population-based stochastic optimization algorithm is used to optimally place the rectangular air regions in the metal plate of a microwave filter. It is shown that the BPF obtained by the proposed method, which has a thin stub, has a desired characteristic. Furthermore, the better performance of the proposed method over the conventional method is confirmed for the design of the BPF with dual peaks.

Index Terms— **Bandpass filters, Geometry projection method, Microstrip filters, NGnet method, Topology optimization.**

I. Introduction

MICROSTRIP LINES (MSLs) are formed by copper foil on the dielectric substrate. Devices consisting of MSLs are widely used in cellular phone base stations and other microwave applications. The rapid growth of communication traffic demands higher performance from these network devices. For this reason, we need effective design methods for circuits using MSLs. In this study, we apply topology optimization (TO) to the design of MSLs. TO searches for the optimal structure by freely deforming the device geometry, which is completely different from conventional design. As a result, TO is expected to yield novel structures with excellent performance. The normalized Gaussian network (NGnet) method is one of the most widely used TO methods. The NGnet method is characterized by its ability to produce smooth shapes, and its effectiveness has been demonstrated in the design of permanent magnet motors, WPT devices and MSLs [1-3].

In the design of MSLs, stubs with elongated conductor shapes are often introduced to cancel the reflected waves, and air gaps with narrowly arranged conductors are also used to create a capacitive effect [4,5]. We call these structures thin structures. Thin structures used for MSL are important for effective design in limited small space. However, because the NGnet method, which represents shapes by superimposing Gaussian functions with concentric circular distributions, tends to produce smooth shapes, it is difficult to represent thin structures such as stubs and air gaps. This difficulty is also shared by the TO methods based on gradient computation [6]. To solve this problem, we introduce a novel TO method that can lead to the thin structures for microstrip devices.

The proposed method is based on the geometry projection method (GPM), which is a TO method that can express shapes with a high degree of freedom by combining simple rectangular or elliptical shapes. The GPM has been applied to the TO of structures called cantilever beams to design light and strong structures [7], resulting in an optimal shape that can be fabricated using off-the-shelf stock material. The second example is a TO based on the GPM of IPM motors with permanent magnets inside the rotor [8], which results in new magnet configurations where the rectangular magnets are randomly generated, and their arrangement evolves to result in high average torque and low torque ripple.

In this paper, we propose a novel method for TO of MSLs based on GPM, which is particularly suitable for the optimization of thin structures required in MSLs. The validity of the proposed method is demonstrated numerically and experimentally. Moreover, the performance of the NGnet is compared with that of the proposed method applied to the TO of MSLs. The main difference from previous studies [7] for a mechanical system and [8] for an electric motor on GPM is that we focus on the generation of thin geometry, which has a significant effect on a microwave device. In addition, we verify the effectiveness of the proposed method by comparing it with experiments that are not included in [7] and [8].

II. Optimization Method

The conductor shape is represented based on GPM as shown in Fig. 1. We randomly place N rectangular discrete elements parameterized by

$$\boldsymbol{p} = (x_1, y_1, w_1, h_1, \dots, x_i, y_i, w_i, h_i, \dots, x_N, y_N, w_N, h_N) \quad (1)$$

in the design region, where x_i and y_i denote the position of the element center, w_i and h_i denote the width and height of the element, respectively. For simplicity, the rotation of the element, which can be introduced if necessary, is not considered in this study. Then, the material attribute M_e of a cell e is determined by

$$M_e = \begin{cases} \text{Air}, & \boldsymbol{x}_e \in \mathcal{D} \\ \text{Conductor}, & \text{otherwise} \end{cases} \quad (2)$$

where $\boldsymbol{x}_e$ denotes the center of the cell e, and $\mathcal{D}$ denotes the collection of the discrete elements. The material attribute M_e is set to air (metal) if the center of the cell is inside (outside) the discrete elements. In a typical setting of GPM, the inside of the discrete element is set to an object such as a conductor. In contrast, the proposed method sets the inside to the opposite, air. This helps to generate a geometry where the ports of the microstrip circuit are connected by conductors. Finally, the optimal shape is obtained by minimizing the objective function. This approach would be effective to represent the thin structure for microwave devices because the shape can be expressed by combining linear structures.

In the optimization, the geometrical parameter vector $\boldsymbol{p}$ is determined to minimize the objective function by the covariance matrix adaptation evolution strategy (CMA-ES) [9], a population-based stochastic optimization algorithm. CMA-ES is good for global search and, in our experience, is often faster than other evolutionary computation methods such as genetic algorithms. During optimization, constraints are imposed on the design variables to ensure that the discrete elements do not exceed the design region, as follows:

$$\begin{cases} X_1 \leq x_i \leq X_2 \\ Y_1 \leq y_i \leq Y_2 \\ s \leq w_i \leq (X_2 - X_1)/2 \\ s \leq h_i \leq (Y_2 - Y_1)/2 \end{cases} \quad (i = 1, \dots, N) \tag{3}$$

where X_1, Y_1 and X_2, Y_2 represent the lower left and upper right coordinates of the design region rectangle shown in Fig. 2, respectively, and s represents the cell size. The parts of the discrete elements that exceed the design region are ignored. If the design variables violate the constraints, the objective function is penalized as follows:

$$F'(\boldsymbol{p}) = \begin{cases} F(\boldsymbol{p}), & \boldsymbol{p} \text{ is feasible} \\ F_p + d(\boldsymbol{p}), & \text{otherwise} \end{cases} \tag{4}$$

$$d(\boldsymbol{p}) = \sum_{i=1}^{4N} \left| p_i - p_0^i \right| \tag{5}$$

where F and F' represent the original and penalized objective functions, respectively, F_p is a penalty constant whose value is greater than the worst objective function value without penalty, d is the distance from the center of the feasible region p_0^i, and p_i denotes the i-th entity of $\boldsymbol{p}$. Since d takes non-negative values, the value of F' when the constraint is violated is always greater than that when it is satisfied, as shown in Fig. 3.

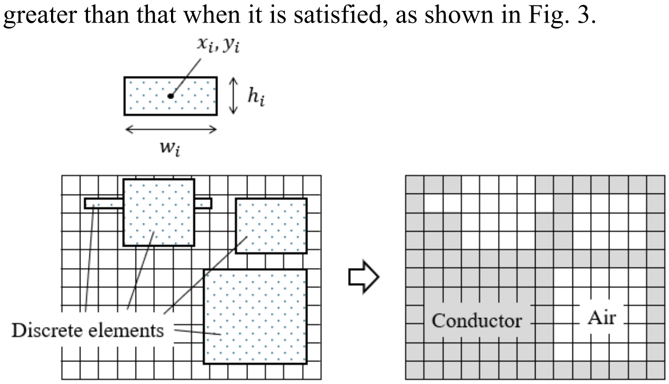

Fig. 1. Schematic of GPM.

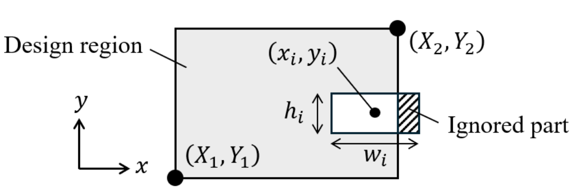

Fig. 2. Optimization constraints and handling of discrete elements outside the design region.

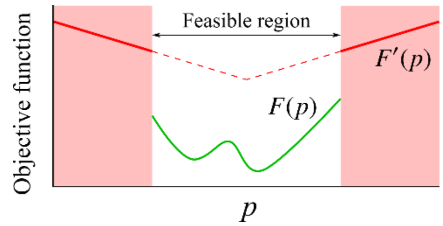

Fig. 3. Objective function with penalty.

III. Design Example for Single-band Bandpass Filter

The optimization model of the microstrip bandpass filter (BPF) is shown in Fig. 4 [3]. The line width of the port is set to 2.295 mm so that its characteristic impedance is 50 Ω. To design the single-band BPF with center frequency $f_1 =$ 2.0 Hz and fractional bandwidth $\Delta_1 = 20\%$, the optimization problem is defined by

$$\text{minimize} \quad F_1(\boldsymbol{p}) \tag{6}$$

$$F_1(\boldsymbol{p}) = \sum_{f \in \text{passband}} S_{21}(f)^2 + \sum_{f \in \text{stopband}} S_{11}(f)^2$$

where S_{ij} denotes the magnitude of the S-parameter, which is evaluated every 0.1 GHz in decibel form, and f is the sampling frequency. The optimization settings are summarized in Table I. The size of the grid mesh in the design region was set to the smallest size feasible for manufacturing. Although an appropriately distributed sampling frequency would improve the optimization, a uniform distribution is assumed here to test the fundamental property.

The optimization took 17 hours 20 minutes for four parallel computations using Intel® Xeon® W-2135 CPU, 3.70GHz. The convergence history is shown in Fig. 5. The MSL is fabricated based on the optimization result as shown in Fig.6. Individuals that satisfy the constraints begin to be generated at around generation 20, and then F_1 rapidly decreases. The optimal F_1 value was 37.7. Fig. 6(b) shows the S-parameters of the optimized shape, with the solid line representing the results measured by network analyzer Agilent E5061B and the dashed line representing the computed results. We find that the two were in approximate agreement. Furthermore, there is a peak of S_{11} in the passband, indicating that the desired characteristics were obtained by the proposed method.

To verify the importance of the thin structure, the original optimized shape was modified by eliminating a thin structure as shown in Fig.7, where the electric field at the stopband ($f = 2.8$ Hz) is also plotted. It can be seen from Fig. 7(a) that the electric field is concentrated on the thin structure, which is considered to act as a resonator. Fig. 7(b) shows that the elimination of the thin structure makes it unable to attenuate the electric field at the output port, despite being in the stopband. In Fig. 7(c), the solid and dashed lines represent the S-parameters of Fig. 7(a) and Fig. 7(b), respectively, indicating that the elimination of the thin structure leads to a significant deterioration of the characteristics. From these results, it is concluded that the thin structure generated by the present TO contributes significantly to the characteristics.

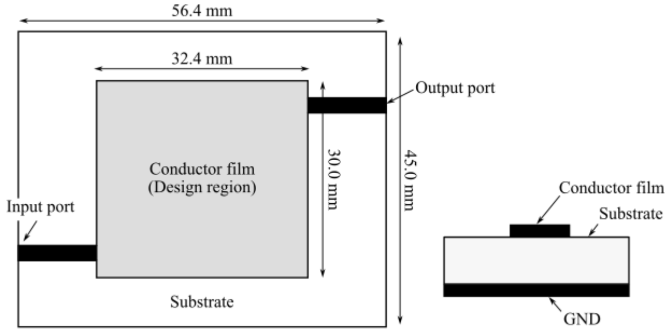

Fig. 4. Top view and cross section of the optimization model [3]. The thickness, relative permittivity, and loss tangent of the substrate are t = 1.2 mm, ε_r = 4.3, and $\tan\delta$ = 0.011, respectively.

TABLE I. OPTIMIZATION SETTINGS

Number of discrete elements N	10
Number of design variables	40
Penalty constant F_p	$70^2 \times 17$
Optimization algorithm	CMA-ES
Population size λ	15
Number of generations	200
Number of grid meshes in design region	432 × 400
Size of grid mesh in design region s	75 µm

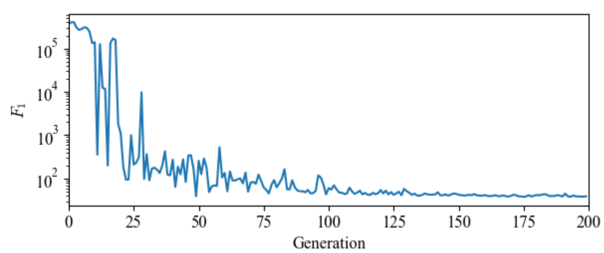

Fig. 5. Convergence history of the objective function F_1.

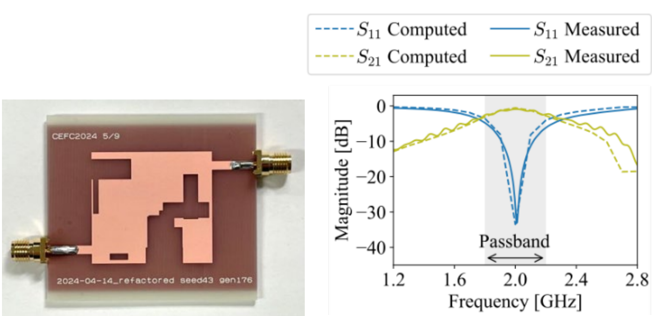

(a) (b)

Fig. 6. Optimization results. (a) Optimized shape and (b) S-parameters. f_1 = 2.0 Hz, Δ_1 = 20%.

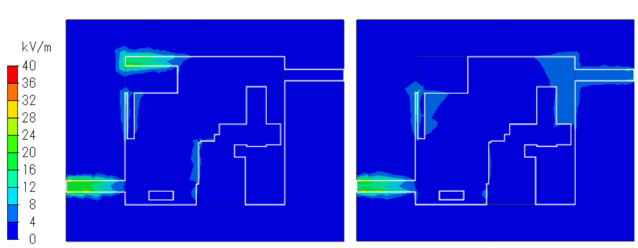

(a) (b)

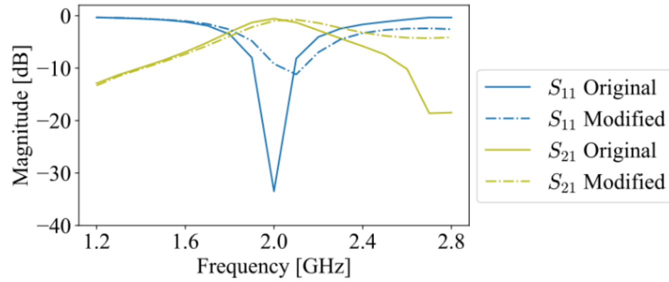

(c)

Fig. 7. Effect of thin stub. Electric fields at f = 2.8 Hz are also shown. (a) Original optimized shape and (b) modified shape where a stub is eliminated. (c) Comparison of the S-parameters for two shapes.

IV. DESIGN EXAMPLE FOR DUAL-BAND BANDPASS FILTER

To demonstrate the advantages of the proposed method over the NGnet method, we design a dual-band BPF, whose optimization would be more difficult than the single-band BPF, using both methods to compare the results. The optimization model is the same as the single-band problem shown in Fig. 4. To design the dual-band BPF with center frequencies f_1 = 2.45 Hz and f_2 = 5.80 Hz, and fractional bandwidths Δ_1 = 12% and Δ_2 = 7% [10], the optimization problem is defined by

$$\text{minimize} \quad F_2(\boldsymbol{p}) \tag{7}$$

$$F_2(\boldsymbol{p}) = k \sum_{f \in \text{passband}} S_{21}(f)^2 + \sum_{f \in \text{stopband}} S_{11}(f)^2$$

where k is the coefficient. Since the number of sampling points in the stopband is about 9 times greater than that in the passband, k = 9 was chosen so that the first and second terms in (7), i.e., the passband and stopband, are evaluated equally. A different value for k may improve the optimization. The design variables and the optimization settings for both methods are shown in Fig. 8 and Table II, respectively. In the NGnet method, the shape is represented by a superposition of Gaussian functions, in which the weighting coefficients $\boldsymbol{w}$ are optimization parameters. In the proposed method, the geometric parameters of the discrete elements to be placed in the design region are again the design variables. Although the shape representations are different for these methods, the number of design variables is set to 36 dimensions for both methods.

The optimization was performed in four parallel computations on Intel® Xeon® W-2135 CPU, 3.70GHz, and took 98 hours 49 minutes for the NGnet method and 54 hours 7 minutes for the proposed method. The convergence histories of the objective function F_2 are shown in Fig. 9. The NGnet method improves F_2 faster in the early generations. The optimization results are shown in Fig. 10. The optimal values of F_2 for the NGnet method and the proposed method were 529 and 477, respectively. In Fig. 10(c) and (d), the S_{11} values resulted from both methods have peaks at the passbands, indicating that they are effective for designing MSLs. There is a small difference between the computed and measured second peaks in (d) probably due to the fabrication errors. On the other hand, the profile between the peaks in (d) is flatter than in (c).

Note that the results shown in Fig. 9 and Fig. 10 are the best results for each method when the optimization is performed two times with different random number seeds. The averages of the F_2 values when the optimization is performed for each of the two methods are 600 for the NGnet method, and 505 for the proposed method. The proposed method improved the F_2 value by 16% on average. It was observed that the NGnet method resulted in many flat elements. This is due to the fact that it tends to generate curved material boundaries. The final results of the NGnet method were obtained by re-generating the mesh after optimization to avoid flat elements. Implicit domain meshing [11], which generates a mesh along the contour line of the shape function, may be effective to avoid the generation of flat elements during the TO process [12]. On the other hand, the proposed method did not generate flat elements even with standard mesh generation method.

V. Conclusion

We have introduced a TO method based on GPM that can lead to thin structures for microstrip devices. The proposed method is adapted from the original GPM to suit microwave device design. The single-band BPF fabricated based on the optimization results has been shown to have the expected frequency characteristics. In addition, the better performance of the proposed method over the NGnet method has been obtained for the design of the dual-band BPF.

References

[1] T. Sato, K. Watanabe, H. Igarashi, “Multimaterial topology optimization of electric machines based on normalized gaussian network,“ in IEEE Transactions on Magnetics, vol. 51, no. 3, 7202604, 2015.

[2] Y. Otomo and H. Igarashi, "A 3-D Topology Optimization of Magnetic Cores for Wireless Power Transfer Device," in IEEE Transactions on Magnetics, 55(6), 8103005, 2019.

[3] T. Jibiki, T. Kawasaki, M. Tanomura and H. Igarashi, "Topology Optimization of Microstrip Lines With Experimental Validation," in IEEE Transactions on Magnetics, 60(3), 7200504, 2024.

[4] D. K. Upadhyay, U. Kumar, G. K. Mishra, and B. L. Shahu, “Design of a Compact UWB Bandpass Filter using Via-Less CRLH TL,” J. Microw. Optoelectron. Electromagn. Appl., vol. 16, pp. 336-350, 2017.

[5] C. C. Chen, Y. R. Chen, and C. Y. Chang, “Miniaturized microstrip crosscoupled filters using quarter-wave or quasi-quarter-wave resonators,” IEEE Trans. Microw. Theory Techn., 51(1), pp. 120-131, 2003.

[6] M. P. Bendsoe and O. Sigmund, Topology optimization: theory, methods, and applications, Springer Science & Business Media, 2003.

[7] J. A. Norato, B. K. Bell, and D. A. Tortorelli, “A Geometry Projection Method for Continuum-Based Topology Optimization with Discrete Elements,” Comput. Methods Appl. Mech. Engrg., vol. 293, pp. 306-327, 2015.

[8] Y. Otomo, T. Abe, H. Igarashi, T. Kato and H. Kurita, "Optimization of Permanent Magnet Configuration Using Boolean Geometry Projection Method for IPM Motors," CEFC2022, Denver, CO, USA, 2022.

[9] N. Hansen, “The CMA evolution strategy: A tutorial,” 2016, arXiv:1604.00772.

[10] J-T Kuo, T-H Yeh and C-C Yeh, "Design of microstrip bandpass filters with a dual-passband response," in IEEE Transactions on Microwave Theory Tech., 53(4), pp. 1331-1337, 2005.

[11] C. Dapogny, C. Dobrzynski, and P. Frey, “Three-dimensional adaptive domain remeshing, implicit domain meshing, and applications to free and moving boundary problems,” J. Comput. Phys., vol. 262, pp. 358–378, 2014.

[12] S.Hiruma, M.Ohtani, S.Soma, S.Kubota, H.Igarashi,Novel hybridization of parameter and topology optimizations: Application to permanent magnet motor. IEEE Trans. Magn., 57(7), 8204604, 2021.

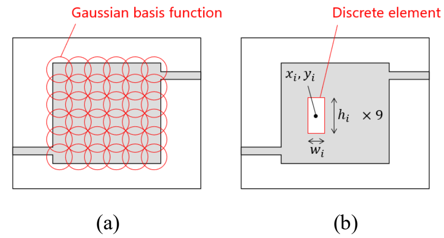

Fig. 8. Design variables for two methods. (a) The NGnet method and (b) the proposed method. Red circles represent the standard deviation of Gaussian basis functions.

TABLE II. Optimization settings

	NGnet method	Proposed method
Number of discrete elements N	–	9
Penalty constant F_p	–	$70^2 \times 71$
Standard deviation of Gaussian basis σ	3.85 mm	–
Number of design variables	36	
Optimization algorithm	CMA-ES	
Population size λ	14	
Number of generations	500	
Number of grid meshes in design region	432 × 400	
Size of grid mesh in design region s	75 µm	

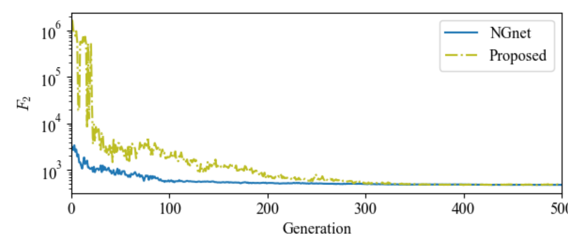

Fig. 9. Convergence histories of the objective function F_2.

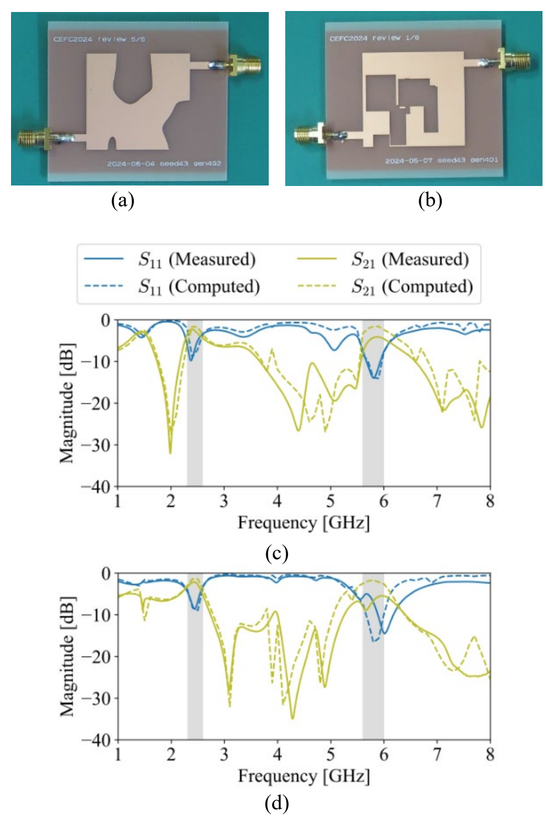

Fig. 10. Optimized shapes and scattering parameters. (a), (c) NGnet ($F_2 = 529$) and (b), (d) proposed ($F_2 = 477$). $f_1 = 2.45$ Hz , $f_2 = 5.80$ Hz , $\Delta_1 = 12\%$, and $\Delta_2 = 7\%$.